

Superconducting Order Parameter Structure in the Nematic Phase of Iron-based Materials

M. M. Korshunov¹⁾, Yu. N. Togushova^{*}

⁺Kirensky Institute of Physics, Federal Research Center

“Krasnoyarsk Science Center of the Siberian Branch of the Russian Academy of Sciences”, 660036 Krasnoyarsk, Russia

^{*}Siberian Federal University, 660041 Krasnoyarsk, Russia

Submitted 28 December 2023

Resubmitted 28 December 2023

Accepted 8 January 2024

We consider the effect of the nematic order on the formation of the superconducting state in iron pnictides and chalcogenides. Nematic order with the B_{2g} symmetry is modelled as the d -type Pomeranchuk instability and treated within the mean-field approach. Calculated nematic order parameter depends on the nematic interaction coefficient and abruptly changes with the coefficient’s increase. The superconducting solution is obtained within the spin-fluctuation pairing theory. We show that the leading solution in the nematic phase has a $s_{\pi\pm}$ structure. From the critical temperature T_c estimations, we conclude that the nematic superconducting state of the $s_{\pi\pm}$ type is more favorable than the usual s_{\pm} and $d_{x^2-y^2}$ type states appearing in the absence of the nematicity.

DOI: 10.1134/S0021364024600046

1. Introduction. Complicated systems are often possess several concurrent or coexisting long range orders of different nature. Iron pnictides and chalcogenides, quasi-two-dimensional systems, are an example. Multiorbital effects there lead to the appearance of an unconventional superconductivity with the order parameter structure of the s_{\pm} type that has the opposite signs at different Fermi surface sheets, still belonging to the A_{1g} representation and being the extended s -wave symmetry [1–5]. Vast amount of experimental data on the superconducting state may be explained within the framework of the spin-fluctuation mechanism of Cooper pairing that, as one of the solutions, has the s_{\pm} state [6]. The presence of this state is confirmed by the data on the spin-resonance peak [7–9] observed in the inelastic neutron scattering [10, 11, 12] and by the observation of the spin exciton characteristic for the s_{\pm} state in the Andreev reflection spectra [13].

Experimentally discovered disparity in the resistance along the orthogonal a and b directions in the iron plane in the tetragonal phase of the iron pnictides [14] led to the conclusion that the C_4 symmetry is broken down to C_2 and the nematic order is formed [15, 16]. The word “nematic” here is used to emphasize that the transition takes place in the electronic subsystem in contrast to the usual structural phase transition with ions mov-

ing to the new equilibrium positions. Close analog is the formation, in the disordered system of spins, of the Ising nematic order with the broken Z_2 symmetry. It is the difference from the usual transition to the magnetic state appearing due to the $O(3)$ symmetry breaking [15]. In other words, nematic phase is characterized by the non-equality in the a and b directions that leads to the inequality of the magnetic response, i.e. the spin susceptibility, in the orthogonal directions in the momentum space, q_x and q_y .

Since with the lowering temperature nematic transition precedes the magnetic or superconducting transitions [17, 18], we study the superconductivity on the background of the already formed nematic order. Here we analyse the role of the Fermi surface symmetry lowering from C_4 to C_2 on the superconducting gap solutions within the spin-fluctuation pairing theory [4]. Resulting solutions have the C_2 symmetry in agreement with the experimentally observed lowering of the gap symmetry [19].

2. Model. We start with the Hamiltonian of the five-orbital model for iron pnictides $H_{5\text{-orb}}$ [20, 21]:

$$H_{5\text{-orb}} = \sum_{\mathbf{k}, \sigma, l, l'} \varepsilon_{\mathbf{k}}^{ll'} d_{\mathbf{k}l\sigma}^\dagger d_{\mathbf{k}l'\sigma}, \quad (1)$$

where $d_{\mathbf{k}l\sigma}^\dagger$ ($d_{\mathbf{k}l\sigma}$) is the creation (annihilation) operator for the electron with the momentum \mathbf{k} , spin σ , and orbital index l , $\varepsilon_{\mathbf{k}}^{ll'}$ is the matrix of the single-electron

¹⁾e-mail: mkor@iph.krasn.ru

energies with the chemical potential being subtracted (diagonal terms) and hopping integrals (off-diagonal elements), which values are presented in [21].

To describe the nematic state, we follow the mean-field approach from [22, 23]. Two-particle nematic interaction gives the following contribution to the Hamiltonian

$$H_{\text{nem}} = -\frac{1}{4} \sum_{\mathbf{k}, \mathbf{k}', \sigma, \sigma', l, l'} V_{ll'}^{\text{nem}} f_{\mathbf{k}l} f_{\mathbf{k}'l'} n_{\mathbf{k}l\sigma} n_{\mathbf{k}'l'\sigma'}, \quad (2)$$

where $n_{\mathbf{k}l\sigma} = d_{\mathbf{k}l\sigma}^\dagger d_{\mathbf{k}l\sigma}$ is the number of particle operator, $V_{ll'}^{\text{nem}}$ are the matrix elements of the interaction, $f_{\mathbf{k}l}$ is the form factor. Following [22, 23] to model the nematic order with the B_{2g} symmetry as the d -type Pomeranchuk instability, we set the form factor to be $f_{\mathbf{k}l} = \cos k_x - \cos k_y$.

To proceed with the mean-field theory, we write the expression $n_{\mathbf{k}l\sigma} = \langle n_{\mathbf{k}l\sigma} \rangle + \delta n_{\mathbf{k}l\sigma}$ with $\langle n_{\mathbf{k}l\sigma} \rangle$ being the average of the occupation number and the deviation from the average $\delta n_{\mathbf{k}l\sigma}$ considered to be small. Inserting the expression into the Hamiltonian H_{nem} , discarding the second order terms by the deviation from the average, and omitting a constant energy shift that would be absorbed into the chemical potential, we derive

$$H_{\text{nem}}^{MF} = \sum_{\mathbf{k}, \sigma, l} \Phi_l f_{\mathbf{k}l} n_{\mathbf{k}l\sigma}. \quad (3)$$

Here we introduced the nematic phase order parameter

$$\Phi_l = -\frac{1}{2} \sum_{\mathbf{k}', \sigma', l'} V_{ll'}^{\text{nem}} f_{\mathbf{k}'l'} \langle n_{\mathbf{k}'l'\sigma'} \rangle. \quad (4)$$

Note that due to the formulation of the two-particle nematic Hamiltonian H_{nem} as the density-density interaction, the mean-field Hamiltonian H_{nem}^{MF} does not contain the interorbital hoppings and describes the changes of the particle density at an orbital l .

3. Nematic order parameter. As the first step, we find the solution for the nematic order parameter Φ_l . To do this, we self-consistently calculate both Φ_l from Equation (4) and the average $\langle n_{\mathbf{k}'l'\sigma'} \rangle$. We set the matrix $V_{ll'}^{\text{nem}}$ to be equal to $\delta_{ll'} V_{\text{nem}}$ with the interaction coefficient V_{nem} . Since it is unknown, we treat it as a parameter. The calculated dependence of Φ_l for different d -orbitals on the coefficient V_{nem} is shown in Fig. 1. Clearly, for small values of V_{nem} nematic state is absent (region I). Order parameter becomes finite once V_{nem} becomes larger than some value, besides, only for one of the orbitals, d_{xy} (region II). Since the value of 4 eV for the interaction coefficient is quite large even compared to the Hubbard repulsion, further we restrict our consideration to regions I and II.

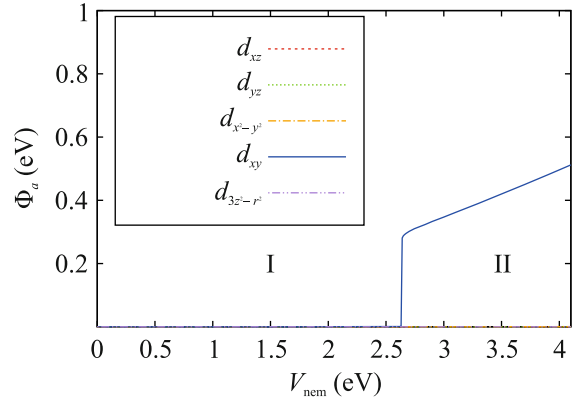


Fig. 1. (Color online) Dependence of the nematic order parameter Φ_a for the orbital a on the interaction coefficient V_{nem} . Roman letters mark the regions where the distinct order parameter behavior is present

Fermi surface and energy dispersion in two different regions are shown in Fig. 2. In the region II ($V_{\text{nem}} = 2.8$ eV), the breaking of the C_4 symmetry held in the region I ($V_{\text{nem}} = 0$) is obvious. This is clearly seen in the dispersion along the $(0, \pi) - (\pi, 0)$ direction.

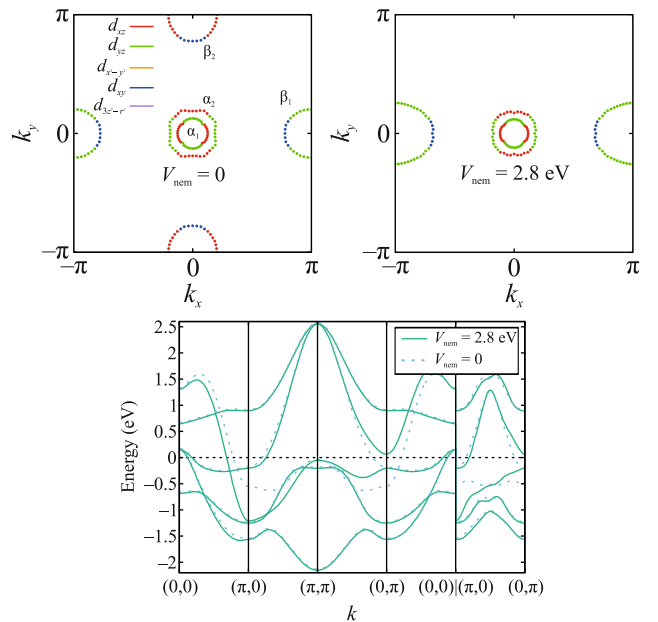


Fig. 2. (Color online) Fermi surface (top) and energy dispersion along the main directions of the Brillouin zone (bottom) for the two values of the interaction coefficient V_{nem} . Energy is shown relative to the chemical potential. $\alpha_{1,2}$ and $\beta_{1,2}$ label the Fermi surface sheets, different colors mark the areas with the maximal contribution from the corresponding orbital

Real part of the dynamical spin susceptibility at zero frequency $\text{Re}\chi(\mathbf{q}, \omega = 0)$ is the central object of the

spin-fluctuation pairing theory [4]. Spin susceptibility is calculated as the spin-spin correlation function

$$\chi^{ll'mm'}(\mathbf{q}, \Omega) = \int_0^\beta d\tau e^{i\Omega\tau} \langle T_\tau S_{ll'}^+(\mathbf{q}, \tau) S_{ll'}^-(\mathbf{q}, 0) \rangle, \quad (5)$$

where Ω is the Matsubara frequency, $\beta = 1/T$ is the inverse temperature, T_τ is the time ordering operator with respect to the Matsubara time τ , S^+ and S^- are the spin operators. Averaging is done over the interacting ensemble. In the zeroth order we have

$$\chi_{(0)}^{ll'mm'}(\mathbf{q}, \Omega) = -T \sum_{\mathbf{p}, \omega_n, \mu, \nu} \left[\varphi_{\mathbf{p}m}^\mu \varphi_{\mathbf{p}l}^{*\mu} G_{\mu\uparrow}(\mathbf{p}, \omega_n) + G_{\nu\downarrow}(\mathbf{p} + \mathbf{q}, \Omega + \omega_n) \varphi_{\mathbf{p}+\mathbf{q}l}^\nu \varphi_{\mathbf{p}+\mathbf{q}m'}^{*\nu} \right]. \quad (6)$$

Here ω_n is the Matsubara frequency, μ and ν are the band indices, $\varphi_{\mathbf{k}m}^\mu$ are the coefficients of the band to orbital transformation, that is $d_{\mathbf{k}m\sigma} = \sum_\mu \varphi_{\mathbf{k}m}^\mu b_{\mathbf{k}m\sigma}$, where $b_{\mathbf{k}m\sigma}$ is the electron annihilation operator in the band basis where the Green's function is diagonal, $G_{\mu\sigma}(\mathbf{k}, \omega_n) = 1/(\omega_n - \varepsilon_{\mathbf{k}\mu\sigma})$.

First we calculate $\chi_{(0)}^{ll'mm'}(\mathbf{q}, \Omega)$ with the Hamiltonian $H_0 = H_{5-orb} + H_{\text{nem}}^{MF}$ and then we get $\chi^{ll'mm'}(\mathbf{q}, \Omega)$ within the random phase approximation (RPA). Ladder approximation, RPA, is constructed with the onsite Coulomb interaction, namely, intraorbital Hubbard U , interorbital U' , Hund's exchange J , and the pair hopping J' [24, 25]. Hamiltonian H_{int} has the following form

$$\begin{aligned} H_{\text{int}} = & U \sum_{f,m} n_{fm\uparrow} n_{fm\downarrow} + U' \sum_{f,m<l} n_{fl} n_{fm} + \\ & + J \sum_{f,m<l} \sum_{\sigma,\sigma'} d_{fl\sigma}^\dagger d_{fm\sigma}^\dagger d_{fl\sigma'} d_{fm\sigma'} + \\ & + J' \sum_{f,m \neq l} d_{fl\uparrow}^\dagger d_{fl\downarrow}^\dagger d_{fm\downarrow} d_{fm\uparrow}, \end{aligned} \quad (7)$$

where $n_{fm} = n_{fm\uparrow} + n_{fm\downarrow}$, $n_{fm\sigma} = d_{fm\sigma}^\dagger d_{fm\sigma}$ is the number of particles operator on the lattice site f .

Sum of the ladder diagrams that include the electron-hole bubble in the matrix form $\hat{\chi}_{(0)}(\mathbf{q}, \Omega)$ gives the following expression for the spin susceptibility matrix in the RPA [4]

$$\hat{\chi}(\mathbf{q}, \Omega) = \left[\hat{I} - \hat{U}_s \hat{\chi}_{(0)}(\mathbf{q}, \Omega) \right]^{-1} \hat{\chi}_{(0)}(\mathbf{q}, \Omega), \quad (8)$$

where \hat{I} and \hat{U}_s are the unity matrix and the interaction matrix in the orbital basis given in [21]. Later we present results for the physical susceptibility $\chi(\mathbf{q}, \Omega) = \sum_{l,m} \chi^{llmm}(\mathbf{q}, \Omega)$ analytically continued to the real frequency axis ω ($i\Omega \rightarrow \omega + i\delta$, $\delta \rightarrow 0+$).

Breaking of the Fermi surface symmetry leads to the lowering of the symmetry to C_2 in the dependence of the spin susceptibility on the wave vector \mathbf{q} . This is shown in Fig. 3. Increase of V_{nem} and the following increase of the order parameter Φ_l leads to the rise of the peak near $\mathbf{q} = (\pi, 0)$ in comparison with $\mathbf{q} = (0, \pi)$. Of course, it is related to the disappearance of the Fermi surface sheets β_2 near $(0, \pm\pi)$, in contrast to β_1 sheets near $(\pm\pi, 0)$. This leads to the dominance of the scattering between the bands forming $\alpha_{1,2}$ sheets and bands forming β_1 sheets in contrast to the bands forming β_2 sheets (see Fig. 2).

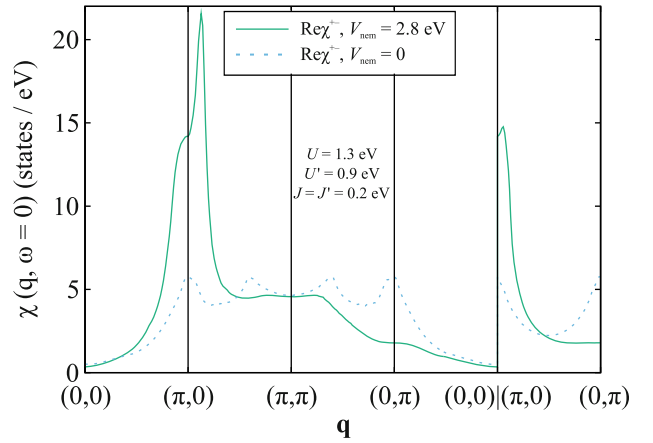


Fig. 3. (Color online) Dependence of the real part of the spin susceptibility at zero frequency on the wave vector \mathbf{q} calculated in RPA for the two values of the interaction coefficient V_{nem}

4. Superconducting state. On the background of the nematic state, we seek for a superconducting state by solving a linearized equation for the order parameter $\Delta_{\mathbf{k}} = \Delta_0 g_{\mathbf{k}}$ written as an equation on the eigenvalues λ and eigenvectors $g_{\mathbf{k}}$ [4, 21, 26–28],

$$\lambda g_{\mathbf{k}} = - \sum_{\nu} \oint_{\nu} \frac{d\mathbf{k}'_{\parallel}}{2\pi} \frac{1}{2\pi v_{F\mathbf{k}'}} \tilde{\Gamma}^{\mu\nu}(\mathbf{k}, \mathbf{k}') g_{\mathbf{k}'}, \quad (9)$$

where $v_{F\mathbf{k}'}$ is the Fermi velocity, the contour integral is taken over the parallel to the ν -th Fermi surface sheet component of momentum \mathbf{k}'_{\parallel} , and the band μ is unambiguously determined by the location of the momentum \mathbf{k} . Positive λ 's correspond to attraction and the maximal one of them represents the state with the highest critical temperature T_c , i.e., the most favorable superconducting state with the corresponding gap function determined by $g_{\mathbf{k}}$.

Cooper vertex $\tilde{\Gamma}^{\mu\nu}(\mathbf{k}, \mathbf{k}')$ depends on the Coulomb parameters U , U' , J , J' and on $\text{Re}\chi(\mathbf{q}, \omega = 0)$, see [4]. Under the spin-rotational invariance assumed here,

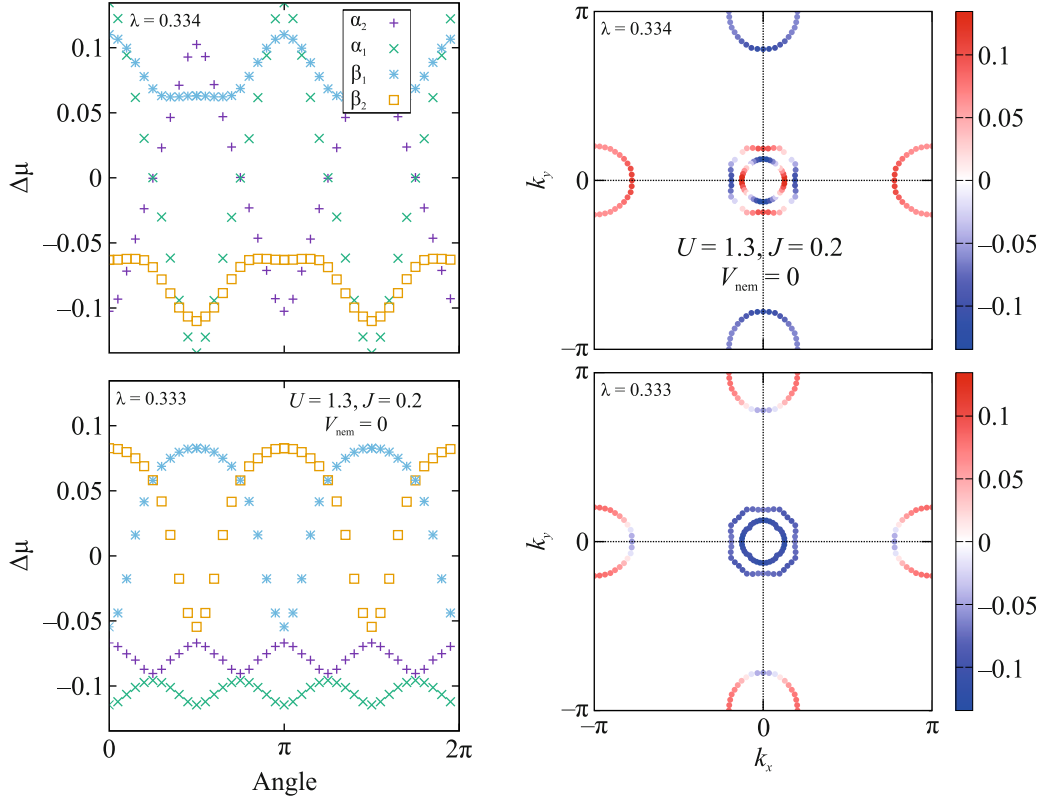


Fig. 4. (Color online) Superconducting order parameter for $U = 1.3$, $J = 0.2$, and $V_{\text{nem}} = 0$ for the two leading eigenvalues λ at the Fermi surface sheets ($\alpha_{1,2}$, $\beta_{1,2}$). Left: angular dependence at each sheet, right: magnitude of the order parameter is shown as the intensity within the Brillouin zone. All values are in eV

$U' = U - 2J$ and $J' = J$. We vary the other two parameters, U and J , of the Hubbard interaction. For the further study we choose the following set of interactions (values in eV)

1: $U = 1$, $J = 0$; 2: $U = 1.1$, $J = 0$; 3: $U = 1$, $J = 0.1$;
 4: $U = 1.2$, $J = 0$; 5: $U = 1.1$, $J = 0.1$; 6: $U = 1.2$,
 $J = 0.1$; 7: $U = 1$, $J = 0.2$; 8: $U = 1.3$, $J = 0$;
 9: $U = 1.1$, $J = 0.2$; 10: $U = 1.3$, $J = 0.1$; 11: $U = 1.4$,
 $J = 0$; 12: $U = 1.2$, $J = 0.2$; 13: $U = 1.4$, $J = 0.1$;
 14: $U = 1$, $J = 0.3$; 15: $U = 1.4$, $J = 0.15$; 16: $U = 1.3$,
 $J = 0.2$.

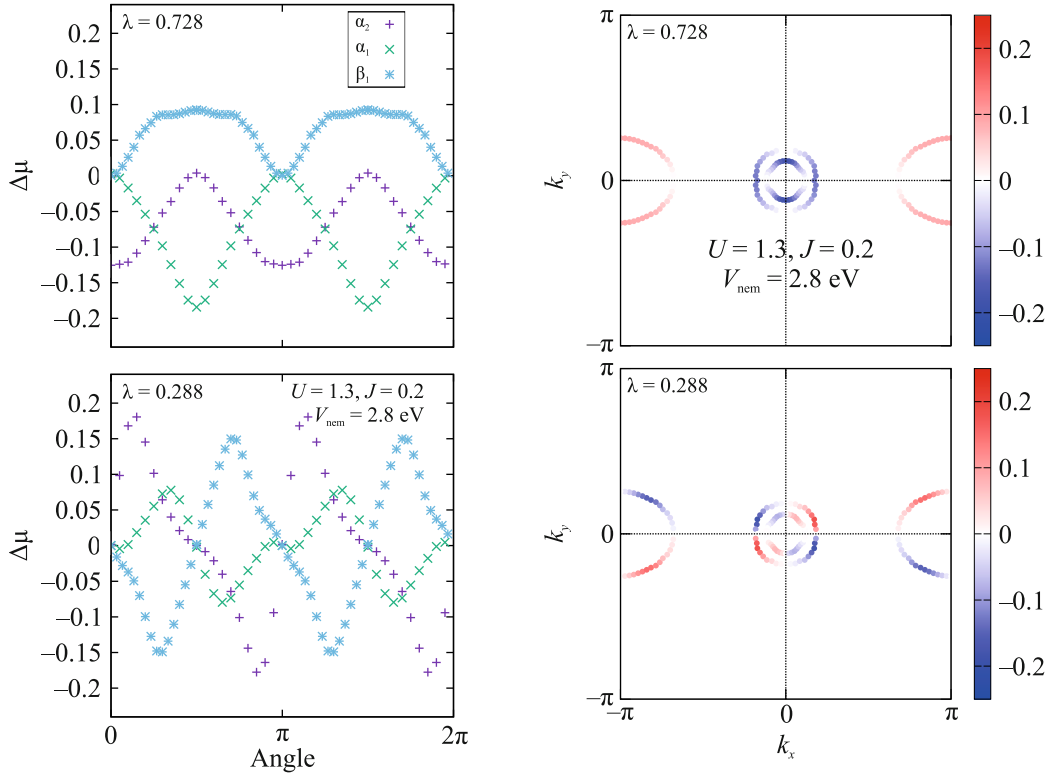
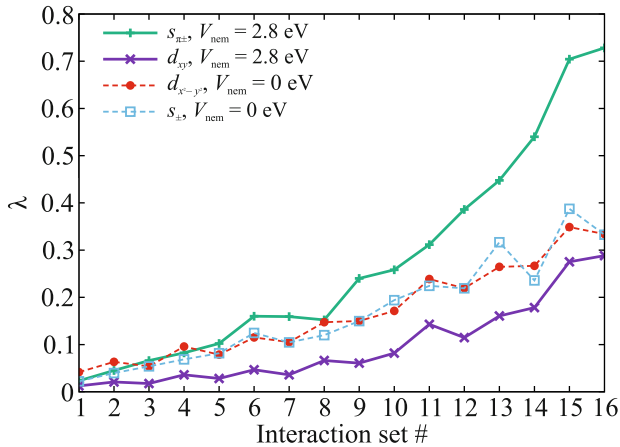
For the set #16 ($U = 1.3$, $J = 0.2$) in Figs. 4, 5, we demonstrate the two solutions of Eq. (9) with the maximal values of λ (leading solutions) in regions I and II: without nematicity at $V_{\text{nem}} = 0$ in Fig. 4 and in the nematic phase at $V_{\text{nem}} = 2.8$ eV in Fig. 5.

For the current set of interaction parameters, $d_{x^2-y^2}$ and s_{\pm} type solutions compete in the region I (i.e., they have close values of λ), however, $d_{x^2-y^2}$ type is winning. In the nematic phase, region II, we can not use the classification of the gaps according to the irreducible representations of the tetragonal phase. Still, we call the state with the larger value of λ in Fig. 5 as “ $s_{\pi\pm}$ ” to em-

phasize its connection to the s_{\pm} state in the tetragonal phase and to point out that the corresponding $\Delta_{\mathbf{k}}$ is invariant under the rotation by π , not $\pi/2$ as was for the extended s -type symmetry. State with the smaller λ in Fig. 5 resembles d_{xy} type symmetry, thus we call it like that.

Combined graph of λ values for the different sets of onsite Coulomb interactions at $V_{\text{nem}} = 0$ and at $V_{\text{nem}} = 2.8$ eV is shown in Fig. 6. Curves correspond to different calculated gap symmetries. Note that the “nematic type” $s_{\pi\pm}$ always has a larger value of λ than the s_{\pm} solution that compete with the $d_{x^2-y^2}$ type. Thus, T_c of the superconducting state coexisting with the nematic state is higher than T_c of the sole superconducting state. This supports the conclusion that the nematic superconducting phase may be more favourable than the state with the unbroken C_4 symmetry.

5. Conclusion. We considered the emergence of the superconductivity on the background of the nematic order in the five-orbital model for iron pnictides and chalcogenides. Nematic order is treated within the mean-field theory with the nematic interaction coefficient V_{nem} . Self-consistently calculated nematic or-


 Fig. 5. (Color online) The same as in Fig. 4 but for $V_{\text{nem}} = 2.8$ eV

 Fig. 6. (Color online) Leading eigenvalues λ for the two values of the nematic interaction coefficient V_{nem} for different sets of Coulomb parameters

der parameter Φ_l is zero (region I) for values of V_{nem} from zero to some critical value, after which the Φ_l component corresponding to the orbital $l = d_{xy}$ unevenly becomes finite (region II). Superconducting solution within the spin-fluctuation pairing theory is found in both regions, I and II. In the absence of the nematic order (region I), the superconducting order parameter has the s_{\pm} and $d_{x^2-y^2}$ type structures for the two leading competing solutions. In the nematic phase

(region II), two leading solutions are of $s_{\pi\pm}$ and d_{xy} types, moreover, first one always wins. Estimation of the corresponding critical temperatures T_c leads to the conclusion that the nematic superconducting state with the $s_{\pi\pm}$ structure will have the higher T_c than the usual s_{\pm} and $d_{x^2-y^2}$ states with the unbroken C_4 symmetry.

Funding. This work was supported within the state assignment of Kirensky Institute of Physics.

Conflict of interest. The authors declare no conflict of interest.

Publisher's Note. Pleiades Publishing remains neutral with regard to jurisdictional claims in published maps and institutional affiliations.

Open Access. This article is licensed under a Creative Commons Attribution 4.0 International License, which permits use, sharing, adaptation, distribution and reproduction in any medium or format, as long as you give appropriate credit to the original author(s) and the source, provide a link to the Creative Commons license, and indicate if changes were made. The images or other third party material in this article are included in the article's Creative Commons license, unless indicated otherwise in a credit line to the material. If material is not included in the article's Creative Commons license and your intended use is not permitted by statutory regulation or exceeds the permitted use,

you will need to obtain permission directly from the copyright holder. To view a copy of this license, visit <http://creativecommons.org/licenses/by/4.0/>.

1. M. V. Sadovskii, *Uspekhi Fizicheskikh Nauk* **178**, 1243 (2008) [M. V. Sadovskii, *Phys. Usp.* **51**, 1201 (2008)].
2. Yu. A. Izyumov and E. Z. Kurmaev, *Uspekhi Fizicheskikh Nauk* **178**, 1307 (2008) [Yu. A. Izyumov and E. Z. Kurmaev, *Phys.-Uspekhi* **51**, 1261 (2008)].
3. P. J. Hirschfeld, M. M. Korshunov, and I. I. Mazin, *Rep. Progr. Phys.* **74**, 124508 (2011).
4. M. M. Korshunov, *Uspekhi Fizicheskikh Nauk* **184**, 882 (2014) [M. M. Korshunov, *Phys.-Uspekhi* **57**, 813 (2014)].
5. M. V. Sadovskii, *Uspekhi Fizicheskikh Nauk* **186**, 1035 (2016) [M. V. Sadovskii, *Phys.-Uspekhi* **59**, 947 (2016)].
6. S. Maiti, M. M. Korshunov, T. A. Maier, P. J. Hirschfeld, and A. V. Chubukov, *Phys. Rev. Lett.* **107**, 147002 (2011).
7. M. M. Korshunov and I. Eremin, *Phys. Rev. B* **78**, 140509 (2008).
8. T. A. Maier and D. J. Scalapino, *Phys. Rev. B* **78**, 020514 (2008).
9. M. M. Korshunov, *Phys. Rev. B* **98**, 104510 (2018).
10. M. D. Lumsden and A. D. Christianson, *J. Phys. Condens. Matter* **22**, 203203 (2010).
11. P. Dai, *Rev. Mod. Phys.* **87**, 855 (2015).
12. D. S. Inosov, *Comptes Rendus Physique* **17**, 60 (2016).
13. M. M. Korshunov, S. A. Kuzmichev, and T. E. Kuzmicheva, *Materials* **15**, 6120 (2022).
14. J.-H. Chu, J. G. Analytis, K. De Greve, P. McMahon, Z. Islam, Y. Yamamoto, and I. R. Fisher, *Science* **329**, 824 (2010).
15. R. M. Fernandes, A. V. Chubukov, J. Knolle, I. Eremin, and J. Schmalian, *Phys. Rev. B* **85**, 024534 (2012).
16. R. M. Fernandes, A. V. Chubukov, and J. Schmalian, *Nat. Phys.* **10**, 97 (2014).
17. J. Li, P. J. Pereira, J. Yuan et al. (Collaboration), *Nat. Commun.* **8**, 1880 (2017).
18. X. Zhou, Y. Li, B. Teng, P. Dong, J. He, Y. Zhang, Y. Ding, J. Wang, Y. Wu, and J. Li, *Adv. Phys. X* **6**, 1878931 (2021).
19. P. O. Sprau, A. Kostin, A. Kreisel, A. E. Bohmer, V. Taufour, P. C. Canfield, S. Mukherjee, P. J. Hirschfeld, B. M. Andersen, and J. C. Seamus Davis, *Science* **357**, 75 (2017).
20. K. Kuroki, S. Onari, R. Arita, H. Usui, Y. Tanaka, H. Kontani, and H. Aoki, *Phys. Rev. Lett.* **101**, 087004 (2008).
21. S. Graser, T. A. Maier, P. J. Hirschfeld, and D. J. Scalapino, *New J. Phys.* **11**, 025016 (2009).
22. H. Yamase, V. Oganesyan, and W. Metzner, *Phys. Rev. B* **72**, 035114 (2005).
23. S. S. Choudhury, S. Peterson, and Y. Idzerda, *Phys. Rev. B* **105**, 214515 (2022).
24. C. Castellani, C. R. Natoli, and J. Ranninger, *Phys. Rev. B* **18**, 4945 (1978).
25. A. M. Oleś, *Phys. Rev. B* **28**, 327 (1983).
26. N. F. Berk and J. R. Schrieffer, *Phys. Rev. Lett.* **17**, 433 (1966).
27. D. J. Scalapino, E. Loh, and J. E. Hirsch, *Phys. Rev. B* **34**, 8190 (1986).
28. M. M. Korshunov, *Itinerant Spin Fluctuations in Iron-Based Superconductors in Perturbation Theory: Advances in Research and Applications*, Nova Science Publishers Inc., N.Y. (2018), p. 61.